MNRAS 000, 1–13 (2023) Preprint 15 September 2023 Compiled using MNRAS LATEX style file v3.0

Panspermia in Star clusters

Ahzam Ahmed K C,[1]★ Richard J.Parker(Supervisor)[2]
[1]Master's Student,Department of Physics and Astronomy,The University of Sheffield, Sheffield S3 7RH, UK
[2]Department of Physics and Astronomy, The University of Sheffield, Hicks Building, Hounsfield Road, Sheffield S3 7RH, UK

15 September 2023

ABSTRACT

We present a study on the lithopanspermia events occurring during the close encounter of two stellar discs. Our primary focus is on understanding the transfer of biologically active entities between these systems. We operate under the assumption that the stellar systems in question are inherently biologically active, making the transferred mass representative of the movement of biologically active entities. Our findings indicate a strong correlation between stellar densities and the amount of mass transferred: higher densities lead to increased mass transfers. Additionally, systems with lower eccentricities also exhibit higher mass transfer. A significant observation is that the majority of encounters and subsequent mass transfers take place within the initial few million years. As time progresses, the frequency of these systems engaging in mass transfer diminishes considerably. In a scenario where the systems are not biologically active, we further explored the potential of these rocks to carry biological entities. Our results suggest that, over the lifespan of a star cluster, it is highly probable for stellar discs to engage in mass transfer during close encounters with other stellar discs.

Key words: Lithopanspermia – Star clusters – Close encounter

1 INTRODUCTION

The origins of life and whether life can spread between celestial bodies have piqued human curiosity for centuries. Panspermia is a predominant theory that posits the interstellar transfer of life. According to panspermia, seeds of life can traverse between planetary systems or other celestial bodies through several mechanisms. Panspermia is classified into various categories depending on the mode of transfer involved. Some of the categories are radio panspermia, directed panspermia, and lithopanspermia. Radio panspermia refers to the process by which seeds of life traverse through space and reach a planet via radiation pressure emanating from stars (Secker et al. 1996), while directed panspermia refers to the deliberate transfer of life to other planets by an advanced civilization (Crick & Orgel 1973). Though these theories remain speculative and difficult to prove with current technology, Lithopanspermia, introduced by Lord Kelvin in 1871 (Wesson 2010), is a modern and more accepted version (Rampelotto 2010). It suggests that life can be transferred between planets via biologically active rocks. According to lithopanspermia, biologically active rocks from a habitable planet get transferred to another planet, and life gets introduced to this new planet. The late 20th century marked a resurgence of interest in this theory, driven by two major discoveries. First, researchers identified microorganisms, like Bacillus subtilis, that have the resilience to survive the harsh environment of space, and thus these organisms can be capable of initiating lithopanspermia (Horneck et al. 1994). Second, the observational detection of rock materials of interstellar origins such as "Oumuamua" and "Borisov" within our solar system proved that the delivery of materials between stellar systems is likely to occur (Meech et al. 2017; Eubanks et al. 2021). Additionally, the discovery of Martian meteorites on Earth provides compelling evidence for material exchange between planets. Some of these meteorites show possible signs of past microbial life, suggesting that if life ever existed on Mars, it could potentially have been transferred to Earth via these space rocks (McKay et al. 1996).

While the concept is intriguing, research has consistently shown that the likelihood of such an occurrence is incredibly low. However, this probability might increase in densely populated cosmic environments. Many of these studies have focused on the transfer of materials within a single planetary system or with celestial bodies within the same stellar system, for which there is more concrete evidence (Worth et al. 2013). The dynamics and feasibility of rocky material transfers between different solar systems, on the other hand, remain a challenging area of study. Estimations have been made, but pinning down precise probabilities is difficult due to the vast distances and variables involved. An essential aspect to consider in lithopanspermia is the survivability of life during interstellar journeys. Rocks carrying biological entities need to be resilient against the hostile conditions of space, which include radiation and extreme temperature fluctuations (Horneck 1993). Based on previous research, it is posited that a rock would need a mass of at least 10 kg to safeguard any biological life within it from the harmful effects of space (Melosh 2003). The primary objective of this research project is to estimate the amount of such rocky material transferred between stellar systems.

The likelihood of lithopanspermia, or the transfer of life-bearing rocks between celestial bodies, significantly depends on the specific dynamical environment in question. Different regions of space exhibit varying degrees of stellar interactions, which directly impact

★ E-mail: ahzamahd641@gmail.com

the feasibility of such transfers. The feasibility of the transfer of materials in different environments, such as the galactic neighbourhood, galactic bulge, old star clusters, and star-forming regions, has been discussed (Gobat et al. 2021; Chen et al. 2018; Belbruno et al. 2012; Adams & Spergel 2005).

Starting with the galactic neighbourhood, we observe a sparse stellar distribution. Here, the stellar number density is a mere 0.1 stars per cubic parsec. Given this low density, the chances of one star interacting with another are slim, making the prospect of mass transfer in such environments nearly negligible. Moving on to star clusters, the scenario changes dramatically. These regions boast a stellar number density ranging from 10 to 10^4 stars per cubic parsec. The increased density means interactions between stars have become commonplace, elevating the likelihood of mass transfer between neighbouring stellar systems. However, the densest of all these environments are the globular clusters. These clusters have an astonishing stellar number density of between 10^3 and 10^9 stars per cubic parsec. At first glance, one might assume that such high densities would lead to frequent stellar interactions and, consequently, higher chances of lithopanspermia. However, globular clusters primarily consist of old, low-metallicity stars. The lack of metals in these stars makes planet formation around them less likely. This factor, combined with their age, diminishes the potential for lithopanspermia, as fewer planets mean fewer opportunities for life-bearing rocks to originate and be exchanged.

The close encounter time between celestial bodies is represented by the equation:

$$t_{\rm enc} = \frac{1}{nC\sigma}$$

$t_{\rm enc}$ is crucial in determining the feasibility of lithopanspermia. Here, 'n' is the stellar number density, 'C' is the capture cross-section, and 'σ' signifies the velocity dispersion. Both number density and velocity dispersion vary across environments, as discussed above. The captured cross-section,

$$C = \pi r^2$$

is another pivotal factor. As 'r' denotes the radius of a stellar cluster, which remains relatively consistent across different environments, the cross-section does not exhibit much variation between galactic fields, star clusters, and globular clusters.

Regions characterised by high stellar density and the presence of young stars, such as embedded star clusters and young star-forming regions, are the most likely places for lithopanspermia to occur, given that life forms quickly. But this may not be the case; however, the material exchange in embedded star clusters and young star-forming regions is higher than in other low-density regions. In these areas, stars often interact with one another, which can impact the protoplanetary discs from which planets emerge. The impact can lead to several changes. Some of the impacts are disc disruptions, The gravitational pull from a passing star can warp, truncate, or even entirely strip away parts of the protoplanetary disk. This can severely hinder planet formation or alter the kinds of planets that form (Parker 2020). The gravitational forces can induce spiral arms in the protoplanetary disk. These arms can lead to regions of enhanced density, potentially speeding up planetesimal formation in those areas (Rice et al. 2004). If the encounter is particularly close or if there's a significant difference in mass between the objects involved, it's possible for planets or other bodies to be captured by the passing star or to be ejected entirely from the system. Such close interactions can dislodge materials from one star's disc, allowing them to potentially become gravitationally bound to a neighbouring star (Jílková et al. 2016). This phenomenon is particularly prevalent in binary star systems, where energy exchanges are most frequent.

In this research project, our primary focus will be to investigate both low-density and high-density stellar environments. Specifically, we aim to determine the extent of mass transfer occurring between star discs within these contrasting settings and understand the dynamics by which these environments facilitate or hinder such transfers. Our focus is on the mass capture occurring between systems during a close encounter. As mentioned above, such a close encounter can dislodge a large number of rocks from one star's disc, get captured, and become gravitationally bound to the close encountering star. By comparing these systems, we hope to discern patterns or trends in mass transfer processes that might be influenced by the stellar density of the environment and the system's inherent eccentricity. We will also analyse how much rock that is being transferred will survive after the simulation timeline. In this research, we are assuming that all the rocks that are being transferred are biologically active and thus we are essentially calculating the amount of lithopanspermia events. Then we will calculate the number of rocks transferred that can be biologically active if the stellar systems initially were not biologically active. Then we will find the minimum disc radius for such a transfer to occur, and finally we will calculate the number of systems that undergo multiple encounters.

2 METHODS, SIMULATIONS AND ANALYSIS

We have used several methods to analyse and study the mass transfer between stellar discs. First, we obtain the data set of a simulation run by my supervisor, Dr. Richard J. Parker. We use this data set to study mass transfer and subsequent studies. The section below will discuss the simulations and analysis we used for this research project.

2.1 Simulation

The vast expanse of the universe is primarily composed of intricate systems where celestial bodies interact through various forces. In this study, we particularly focus on the evolution of stars within dense star clusters and regions with lower density. Here 'low density' represents a stellar environment with a density of 100 solar masses per cubic parsec, such as the Taurus region. Conversely, 'high density' refers to a stellar environment with 10^4 solar masses per cubic parsec; these densities are seen in Orion Nebula Cluster (ONC) (Parker 2014). Such regions can be efficiently modelled using N-body systems, where each "body" represents a star. These stars influence each other mainly through gravitational attraction. Broadly, these systems can be categorised into collisional and collision-less types. In a collision-less system, the overarching gravitational effects of a large number of particles can be averaged out, making direct interactions between individual particles negligible. However, our study pertains to collisional systems, where these individual interactions are pivotal. In such systems, the gravitational influence between individual stars significantly alters their trajectories. The cumulative effect of these interactions over time plays a decisive role in shaping the fate of the entire star cluster. To generate the requisite data for this study, we employed the Hermite scheme for N-body simulations. The Hermite scheme is a fourth-order, non-symplectic integrator. Hermite schemes are regarded as non-symplectic integrators because they do not have the built-in mechanism to inherently conserve the energy (Hamiltonian structure) of the system over long simulations, which is a hallmark of symplectic integrators. The Hermite integrator is tasked

with forecasting the future positions and velocities of the N-bodies within the star cluster (Dehnen & Read 2011).

The Hermite scheme stands out in the domain of computational methods, particularly for its use of Taylor expansions to accurately describe the positions and velocities of celestial bodies. Its fourth-order precision distinguishes it from many other methods, offering an enhanced accuracy that is crucial when studying the vast expanse of the cosmos. Dehnen & Read (2011) provides a mathematical representation derived from the Taylor expansion for a given time $t + deltat$, we have:

$$x_1 = x_0 + \frac{1}{2}(\dot{x}_1 + \dot{x}_0)\Delta t + \frac{1}{12}(a_0 - a_1)\Delta t^2 + O(\Delta t^5) \quad (1)$$

$$x_1 = \dot{x}_0 + \frac{1}{2}(a_1 + a_0)\Delta t + \frac{1}{12}(\dot{a}_0 - \dot{a}_1)\Delta t^2 + O(\Delta t^5) \quad (2)$$

Here, x_1 and $\dot{x}_1$ represent the updated position and velocity, respectively. Meanwhile, x_0 and $\dot{x}_0$ denote the initial position and velocity. The terms a and $\dot{a}_0$ correspond to acceleration and jerk, with the latter quantifying the rate of change in acceleration. It's essential to note that the calculations involved in determining x_1 and x_2 are not straightforward. Dehnen & Read (2011) in their publication, delve into the complexities associated with these computations. They also elucidate the potential pitfalls and the strategies adopted to address these challenges, ensuring that the Hermite scheme's results remain robust and reliable.

The N-body simulations, integral to this study, were conducted by my supervisor, Dr. Richard Parker. Through these simulations, we aimed to gain insights into the dynamics of close encounters between stars and understand the transfer of mass during these interactions. For the purposes of our analysis, we used data sets from a total of 30 simulations. There were 3 sets of initial conditions and 10 versions of each initial condition, for a total of 30 N-body simulations. These data sets are bifurcated based on three unique environmental conditions to ensure a comprehensive understanding.

(i) **High Stellar Density, Short Duration:** This subset contains 10 simulation data sets, each representing a high stellar density environment. Every simulation in this category was run for a duration of 10 million years. The stellar density at time zero is 10,000 solar masses per cubic parsec.

(ii) **Low Stellar Density, Short Duration:** 10 simulation data sets fall into this category. Contrary to the previous set, these simulations represent a low stellar density environment but maintain the same runtime of 10 million years. The initial stellar density is 100 solar masses per cubic parsec.

(iii) **High Stellar Density, Long Duration:** The remaining 10 simulations also represent a high stellar density environment, akin to the first subset. However, these simulations were run for a more extended period of 100 million years, allowing for a deeper exploration of long-term stellar interactions. The initial stellar density is 10,000 solar masses per cubic parsec.

One of the pivotal attributes of this data is the detailed record of close encounters between stars throughout the duration of each simulation. This enabled us to delve deeper into the dynamics and consequences of such encounters in various environmental conditions.

The simulation of star clusters is set up using the fractal distribution method of Goodwin & Whitworth (2004). While their paper delves deeply into the methodology, a concise overview is as follows: The simulation is set up by starting with a large cube and placing an initial star at its center. This cube is then divided into smaller sections, with each section containing a star. Some of these stars are then randomly chosen to "grow up" and have their surrounding space further subdivided, adding more stars in the process. To prevent the cluster from appearing overly structured, the positions of stars are slightly randomised (Goodwin & Whitworth 2004). The distribution of these stars, either densely packed or spread out, is governed by a value called the fractal dimension D. The fractal distribution can range from $D = 1.6$ to $D = 3$, with $D = 1.6$ representing a highly substructured distribution and $D = 3$ representing a uniform distribution. Thus, a smaller fractal dimension translates to a more pronounced substructure within the cluster (Parker 2014). In our simulation model, stars are assigned masses based on the Maschberger Initial Mass Function (IMF), with a range spanning from 0.01 to 50 solar masses (Maschberger 2013). This mass distribution is key to understanding the dynamics and evolution of the simulated star clusters. The movement of the stars within these clusters follows observed astrophysical patterns: stars in close proximity to one another exhibit almost the same way, while those spaced farther apart display distinct velocities. As for their initial distributions, the stars are distributed in a highly substructured manner, guided by a fractal distribution with a dimension, $D = 1.6$. As the simulation progresses, these star-forming regions undergo dynamic relaxation. Despite their initial subvirial state, they are drawn into the gravitational potential well, culminating in the emergence of a smooth, centrally-focused star cluster. The time required for this transformation is contingent on the initial density of the star-forming region. A detailed visual representation of the transition from initial to final states in both high-density and low-density setups can be observed in figures 1,2 and 3.

Figure 1 Series: This series focuses on a high-density stellar environment over a span of 10 million years. In figure 1(a), we observe the initial conditions, where the distribution of stars is shown at the starting point, time zero. By the time we reach figure 1(b), the simulation has advanced to 3 million years, showcasing the progression in the positioning of stars at this time. The series culminates with figure 1(c), which presents the distribution of stars at the end of the simulation, at 10 million years.

Figure 2 Series: This set of graphs delves into the dynamics of a low-density stellar environment over the same 10-million-year time frame. figure 2(a) depicts the beginning state of the simulation. Moving on to figure 2(b), we can see the state of the stars' distribution after 3 million years. The final state of this environment, after 10 million years, is portrayed in figure 2(c).

Figure 3 Series: In this series, the emphasis is on a high-density stellar environment, but the time frame is extended to 100 million years. figure 3(a) represents the initial stellar distribution at the outset of the simulation. As the simulation evolves, 3(b) highlights the stellar positions at 30 million years. Finally, 3(c) gives us a glimpse into the long-term evolution by presenting the distribution of stars at 100 Myr.

We use a schematic illustration based on Figure 2 from Parker (2014) to comprehend the evolution of the cluster. As depicted in Figure 4 , the blue line represents the density evolution of a high-density stellar environment, while the orange line portrays the evolution in a low-density setting. Initially, the high-density environment exhibits a stellar density of 10^4 solar masses per cubic parsec, significantly greater than the low-density environment's modest 100 solar masses per cubic parsec. However, by the conclusion of the simulation at 10 Myr, both environments converge to a similar stellar density. This convergence is attributed to the accelerated expansion exhibited by clusters with higher densities. This can also be noted from the axis values of Graph 1. Specifically, in the 10 Myr high-density simulation, there's a substantial expansion of the axes after just 3 million

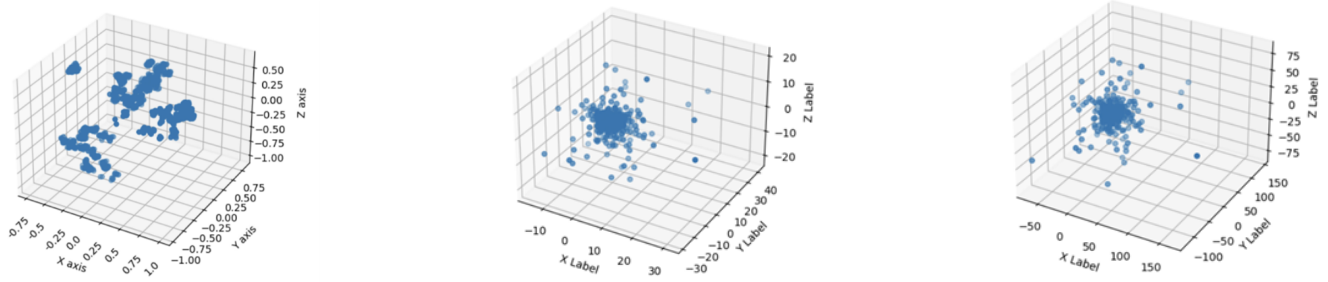

1 (a) 1 (b) 1 (c)

Figure 1. Figure 1(a), 1(b) and 1(c) illustrate the distribution of stars for a high density environment. 1(a) represents the initial substructure of the simulation, 1(b) plots the distribution after 3 Myrs and 1(c) plots the distribution at the end of the simulation.

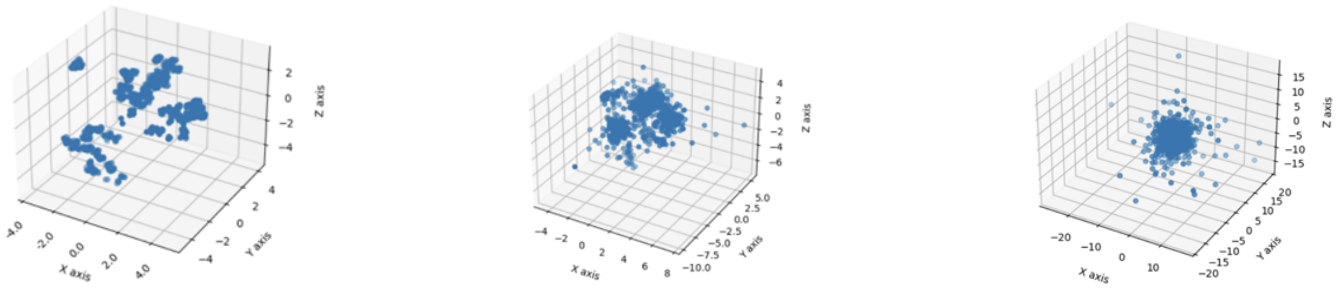

2 (a) 2 (b) 2 (c)

Figure 2. Figure 2(a), 2(b) and 2(c) illustrate the distribution of stars for a low density environment. 2(a) represents the initial substructure of the simulation, 2(b) plots the distribution after 3 Myrs and 2(c) plots the distribution at the end of the simulation that is 10 Myrs.

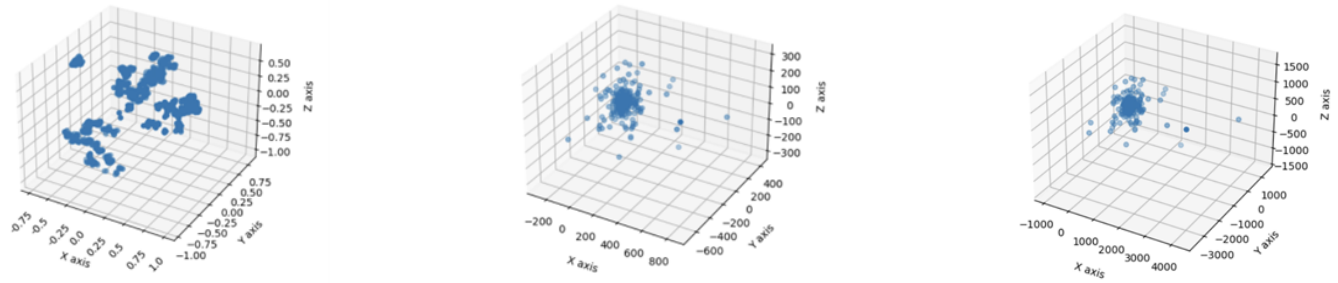

3 (a) 3 (b) 3 (c)

Figure 3. Figure 3(a), 3(b) and 3(c) illustrate the distribution of stars for a high density environment but the simulation runs for a longer time. 3(a) represents the initial substructure of the simulation, 3(b) plots the distribution after 30 Myrs and 3(c) plots the distribution at the end of the simulation that is 100 Myrs.

years. This expansion is notably larger than what's observed in the low-density setting during the same timeframe. This phenomenon suggests that in high-density environments, stars tend to disperse over vast distances over time, leading to a corresponding increase in the x, y, and z axes.

2.2 Close encounter distribution

Close encounters between stars play a pivotal role in the dynamics of protoplanetary discs, where planets are born. Such encounters can significantly alter these discs, leading to the potential exchange of mass between neighbouring stars. Figure 5 illustrates the distribution of these close encounters between the different stellar environments in our simulation data set. For this study, a 'close encounter' is defined as an instance where two stars approach within a distance of 1000 astronomical units (AU) from each other. As our data elucidates, the frequency of these close encounters isn't uniformly distributed. Dense stellar environments, predictably, witness a higher frequency of such events. This serves to reinforce the conception that areas with a high concentration of stars become conducive zones for mass exchange. On the contrary, stars located in sparser, low-density regions experience fewer close encounters. Given the increased interactions in denser environments, the chances of interstellar exchanges of life-bearing materials are considerably higher. In contrast, stars in low-density environments have fewer close encounters, reducing both the potential for mass transfer and the likelihood of lithopanspermia. Figure 5 amalgamates data from all 30 simulation sets. A discerning observation reveals that in the simulations mimicking high-density

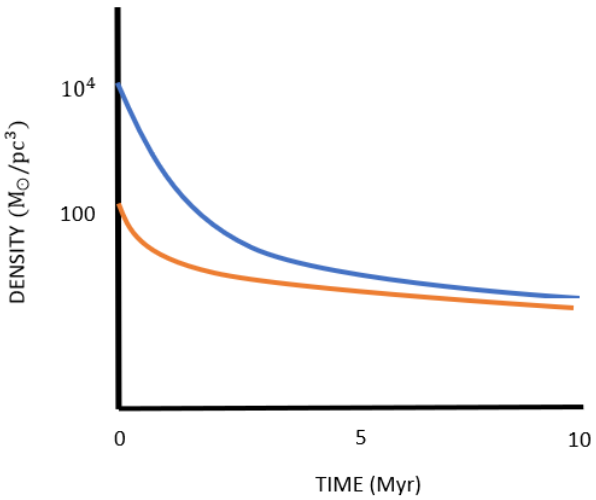

Figure 4. This is a depiction of how evolution of cluster happens with time for different stellar densities. The blue line depicts the high density cluster while orange line depicts the low density region of our simulation.

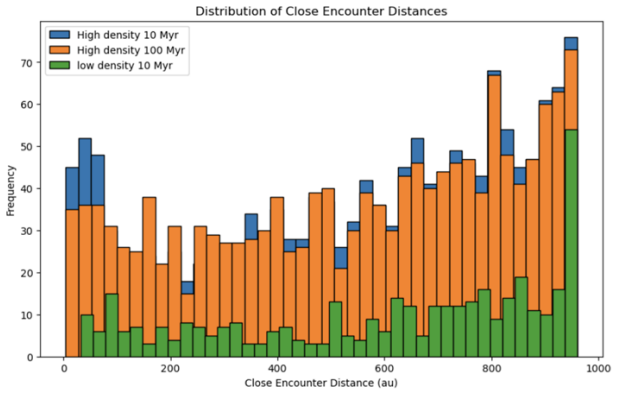

Figure 5. Close encounter distribution over close encounter distance for different stellar densities.

environments, 1, 150 stars out of the total had at least one encounter with another star. Meanwhile, in simulations that replicated low-density conditions, only 560 stars underwent close encounters over the simulation period. This stark difference not only shows how important the density of the environment is in how stars interact, but it also tells us a lot about how these stellar systems might have changed over time.

2.3 Binary star counts

We derived the binary stars from our dataset through a systematic method. Initially, we identified mutual nearest neighbours star systems by employing the K nearest neighbour algorithm. To ascertain whether two mutual nearest neighbours are a binary, we used the binding energy equation:

$$E_{\text{total}} = \frac{M_1 M_2 (V_1 - V_2)^2}{2(M_1 + M_2)} - \frac{G r_1 r_2}{M_1 + M_2} \tag{3}$$

Where, M_1 and M_2 are the masses of the mutual nearest neighbouring stars, v_1 and v_2 are the velocities, and r_1 and r_2 are the positions of the mutual nearest neighbouring star systems.

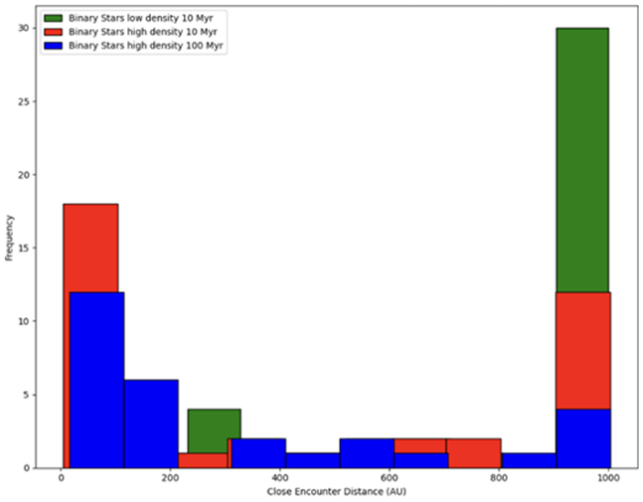

Figure 6. Number of binary stars for different stellar density environments

If the calculated binding energy is negative, it indicates that the star system is a binary.

Our findings, illustrated in figure 6, showcase the distribution of binary stars alongside their close encounter distances. A notable observation from our analysis is that low-density environments exhibit a higher number of binary stars. This trend can be attributed to the dynamics in denser environments where star systems frequently undergo gravitational interactions with neighboring stars. Such interactions in dense settings heighten the risk of disrupting established binary systems, subsequently leading to a reduced count of binary stars in these regions (Pang et al. 2023).

2.4 Calculation of transferred Mass

In the study conducted by Jílková et al. (2016), the transfer efficiency of materials between stellar discs was evaluated. By examining figures 8 and 9 from their paper, we extracted data on transfer efficiency values associated with varying close encounter distances and mass ratios between the two stars. Using these values, a linear regression model was employed to predict the transfer efficiency for our specific set of close encounter distances and mass ratios. We calculate the transfer efficiency when the eccentricity of the encounter is 1 and when eccentricity is 3.5. The associated Python code for this calculation can be found in Appendix A.

The transfer efficiency, denoted by μ_{tr}, represents the ratio of the total number of transferred particles to the total initial number of particles in a star. Mathematically, this can be written as:

$$\mu_{tr} = \frac{m}{0.1 \times M} = \frac{m}{M_{\text{disc}}} \tag{4}$$

Where n is the number of particles transferred, N is the total number of initial particles, m is the mass of transferred particles, and M is the total mass of particles.

Our primary focus is on the mass transfer that occurs within the discs of stars, which predominantly comprises dust when the debris disc is young, while for older debris discs dust content is low. Dust within these star discs is vital as it represents the solid content or rocky materials and serves as the foundational blocks for planet formation. However, it is essential to understand that a protoplanetary disc's mass isn't entirely made up of dust. In fact, it's primarily gaseous. The mass distribution in a star disc typically has a gas to dust ratio of 100:1.

To contextualize this, consider the disc mass of a star, which is approximately 10% of the star's mass, denoted by $M_{\rm disc}$. Given that the gas to dust ratio is 100:1, the dust mass $M_{\rm dust}$ is 1% of $M_{\rm disc}$, or mathematically:

$$M_{\rm dust} = 0.01 \times M_{\rm disc} \tag{5}$$

Given this, our transfer efficiency equation can be refined to:

$$\mu_{tr} = \frac{m}{M_{\rm disc}} = \frac{m}{M_{\rm dust}} \tag{6}$$

Finally, the total transferred mass between stellar systems is given by:

$$m = M_{\rm dust} \times \mu_{tr} \tag{7}$$

This gives us the total biologically active mass transferred between two stellar systems or the total lithopanspermia mass transferred between systems during a close encounter.

2.5 Fraction of rocks that are suitable for lithopanspermia

In the preceding sections, our mass transfer computations were largely grounded on the premise that the star systems facilitating mass transfer were already biologically active. In other words, we've been focusing on quantifying lithopanspermia events based on this presumption. However, to broaden our scope and accommodate a more inclusive perspective, let's momentarily set aside that assumption. Instead, we will calculate the number of rocky materials that meet the requisite criteria to potentially harbour life, thereby enabling lithopanspermia. This assumes that the interacting star systems might not necessarily be biologically active at the onset. A crucial factor that comes into play here is the resilience of these rocks. To ensure that any potential biological entities remain shielded from the often-hostile interstellar environment, a rock would need to have a minimum mass of 10 kg.

We use a specific equation proposed by Adams & Napier (2022) to extrapolate the total number of such capable rocky materials with a mass greater than 10 kg:

$$N_{\rm Litho} = \frac{(2-p)}{(p-1)} \left(\frac{m_1}{m_2}\right)^{p-1} \frac{M_R}{m_2} \tag{8}$$

Where: p is the power-law index, indicative of the mass distribution of transferred rocks. For our considerations, p is assigned a value of $\frac{5}{3}$. M_R signifies the total mass that undergoes transfer during the interaction. m_1 corresponds to the lower mass boundary of the rocky materials, which is set at 10 kg. m_2 represents the upper mass threshold. We assume that the heaviest rock involved in a mass transfer cannot exceed 10% (or 0.1 times) of M_R. This premise is rooted in the logic that it's improbable for a singular rock to constitute a major portion of the total transferred mass during any given event.

With this, we can now ascertain the total number of rocks transferred between stellar disks that have the potential to sustain life.

2.6 Fraction of active materials at the end of the simulation

Having identified the total count of rocky materials available for harbouring biologically active organisms, we then focused on estimating the survival rate of these materials at the culmination of our simulation. This aspect is crucial, as understanding the survival of these biologically active rocks in a stellar system provides insights into the potential longevity of life-bearing materials in the cosmos. To quantify this survival rate, we used relations derived from Adams & Napier (2022). Their research provides a mathematical fit that quantifies the fraction of celestial bodies that remain anchored within a stellar system post-capture, with this fraction evolving as a function of time. This time-dependent fraction is denoted as $F(t)$. The mathematical representation for $F(t)$ is articulated as:

$$F(t) = \frac{1}{1 + \left(\frac{t}{\tau}\right)^{\frac{8}{5}}} \tag{9}$$

Here, t symbolises time, while the timescale τ is defined as 0.84 Myr, which is a typical time over which a significant fraction of captured objects is lost. We calculate the total number of surviving objects at the end of our 10 million-year simulation and our 100 million-year simulation. We will discuss this in detail in the result section.

2.7 Minimum disc radius for mass transfer

Jílková et al. (2016) introduced a formula to compute the minimal disc radius from which particles can be transferred between stars. This radius, denoted as $r_{\rm un,min}$, represents the innermost boundary in a stellar disc from which material can be exchanged between stellar systems. The equation for this is:

$$r_{\rm un,min} \approx \alpha \left[\left(1 + \frac{M_1}{M_2}\right)(1 + e_{\rm enc})\right]^{\left(-\frac{1}{3}\right)} q_{\rm enc} \tag{10}$$

Where: $r_{\rm un,min}$ is the minimal disc radius required for the transfer of particles between stars. α is a factor contingent on the encounter type. It is approximately 0.3 for a prograde encounter (where the two stars move in the same rotational direction) and 0.5 for a retrograde encounter (where the stars move in opposing directions). M_1 and M_2 represent the masses of the two interacting stars. $e_{\rm enc}$ is the eccentricity of the disc particles, which gives an indication of how elongated the orbit of these particles is. $q_{\rm enc}$ is the close encounter distance. By altering the parameters in the equation, different values of $r_{\rm un,min}$ can be derived. A comprehensive exploration of these variations and their implications will be detailed in the results section.

2.8 Chain of encounters

We are calculating the number of lithopanspermia events occurring between stellar systems when encounters between two stars occur during the course of the simulation, which is between 10 million and 100 million years. It is possible that during the course of the simulation, multiple encounters or a chain of encounters can occur. If such a chain of encounters occurs, then it is possible that the biologically active rocks can be transferred between multiple systems. For example, star 1 has an encounter with star 2 at 1 million years old, and N amounts of rocks are transferred. Star 2 has an encounter with Star 3 at 2 million years old, and another N amount of rocks are transferred. Then it is possible that the mass transfer from star 2 to star 3 also contains rocks from star 1, due to its encounter with star 2 at an earlier time. We calculate the number of such chains of events occurring, and the details are given in the result section. The code used to identify the chain of encounters is given in the appendix.

3 RESULTS

In each simulation, we calculate the total number of encounters occurring, how they differ between different stellar environments, and how the encounter varies with time. We then calculate the minimum disc radius required for the transfer of mass between stellar systems to

occur. We then identify the encounter systems where the disc radius is greater than the minimum disc radius for transfer, as only in these systems will mass transfer occur. We then calculate the transferred mass between stellar discs during a close encounter and how much of these rocky materials are suitable for carrying life during the simulation if, initially, the star systems are not biologically active. We finally calculate the fraction of materials that will remain at the end of the simulation, and we also identify the stellar discs that can have a chain of encounters.

3.1 Close encounters

Figure 7(a), 7(b) and 7(c) depict the close encounter distance vs close encounter time distribution for all our simulations. Figure 7(a) and 7(b) plots the close encounter distance vs close encounter time distribution for high density environment and low-density environment respectively. Figure 7(a) plots a high-density environment and we observe that most of the encounters happens at an early period. This indicates that in high-density regions, encounters between stellar objects occur more frequently. Converesly, in panel (b), we see that the close encounter times here are substantially longer in the lower-density simulations. This illustrates that in low-density regions, encounters are less frequent, Both the graphs 7(a) and 7(b) show the encounters occurring during the first 10 million years of the simulation. Graph 7(c) shows the encounters occurring after 10 million years till 100 million years in the high-density simulations. From this graph we see that the number of encounters after 10 million years is low. This variation has a profound impact on our understanding of material transferred between stars. In high density regions where stars undergo frequent close encounters, there is a higher likelihood of materials being exchanged between them. In contrast, in the low-density regions, the infrequency of encounters makes material exchange between stars much less likely. Similarly, most of the encounters occur during the first million years, indicating that most material transfer occurs during the young ages of a few million years.

3.2 Mass transferred during encounter

Graphs 8(a), 8(b), and 8(c) show the cumulative mass exchanged between stellar discs during their proximate interactions. Drawing from data in Graphs 8 and 9 of Jilkova et al., we formulated an equation to represent this mass transfer, expressed as $m = M_{dust} \times \mu_{tr}$. Herein, m signifies the aggregate mass exchanged between the discs, with M_{dust} denoting the dust mass within the disc and μ_{tr} representing the transfer efficiency. Our findings underscore the influence of encounter eccentricity on mass transfer, particularly at values of 1 and 3.5. Notably, systems with smaller eccentricities, as highlighted by the blue bar, exhibit a heightened propensity for mass transfer. The frequency of such transfers peaks at a few 10^{26} kg for an eccentricity of 1, whereas it remains slightly below 10^{26} kg for an eccentricity of 3.5. This trend persists in Graph 8(b), which focuses on environments characterised by low density. The frequency axis of this graph reveals a reduced number of encounters in these environments, implying fewer systems capable of significant mass transfer. However, the peak mass transfer in such low-density settings mirrors that observed in high-density environments. This suggests that while high-density environments witness a greater number of encounters and subsequent mass transfer events, the amount of mass exchanged remains consistent across both high- and low-density settings. Graph 8(c) shows the results for transfer between 10 million and 100 million years for a high-density environment. After the initial 10 million years, the frequency of stellar encounters diminishes considerably. Yet, the peak mass transferred during these sporadic interactions surges, indicating that while mass transfer events between 10 and 100 million years are less frequent, the volume of mass exchanged in each instance is higher. Specifically, for encounters within this period, the mass transfer peaks at 10^{27} kg for an eccentricity of 1 and at several 10^{26} kg for an eccentricity of 3.5. This can be due to several reasons. Stellar systems undergo a series of evolutionary changes over their lifetimes.

3.3 No of suitable rocks that can carry biologically active entities

In the previous section, we explored the complex mechanics of mass transfer between stellar discs during close encounters. Building on that understanding, this section narrows its focus to the quantification of rocky materials that can potentially support biological activity. A significant distinction here is that while our earlier discussions assumed transferred masses between stellar systems to be biologically active, we abandon that assumption in this segment. Instead, we operate under the assumption that not all mass transfers between these stellar systems are biologically active. Our objective now shifts to identifying the number of rocks capable of carrying biologically active materials, regardless of whether they currently do. A critical criterion for these rocks is a mass exceeding 10 kg. This ensures that the rock can effectively shield any biological entities it might carry from the harmful effects of space, creating a haven for potential life forms. This number, NR, represents the total quantity of rocks suitable for lithopanspermia, underlining its significance in our study.

Section 2.5 describes the methodologies we employed to determine the count of these potentially biologically active rocky materials, henceforth referred to as NR. The mathematical representation for NR is articulated in the methods section. This equation is influenced by a number of factors and is expressed as:

$$NR = \frac{(2-p)}{(p-1)} \left(\frac{m_1}{m_2}\right)^{p-1} \frac{M_R}{m_2} \tag{11}$$

In this equation, the variable p represents a power law index. For our calculations, we adopt a value of 1.8 for p, which aligns with empirical observations for collisional systems. The essence of the NR equation is its ability to compute the quantity of materials within a specified mass range as a fraction of the total transferred mass. Specifically, our analysis targets materials with masses ranging from 10 kg up to 0.1 times the total mass transferred. The mass limit of 10 kg is taken because previous studies indicate a rocky material should be at least 10kg in mass in order for the biological organisms in the rocks to survive the harmful effects of radiation.

Our findings, encapsulated in Figure 9 and Table 1, offer a comprehensive overview of the number of rocky materials transferred across diverse environments, eccentricities, and timeframes. The graph juxtaposes two distinct scenarios: a high-density environment and its low-density counterpart. While a cursory glance might suggest a negligible difference in the number of biologically viable rocks transferred between these environments, from Table 1, we can understand it better. Table 1 provides a detailed breakdown of material transfer across different time intervals, specifically focusing on the influence of environmental density and eccentricity. It categorises the data into two primary environmental densities: high and low. Within each density category, the material transfer is further differentiated based on two distinct eccentricities: 1 and 3.5. For the high-density environment with an eccentricity of 1, the material transfer starts at a

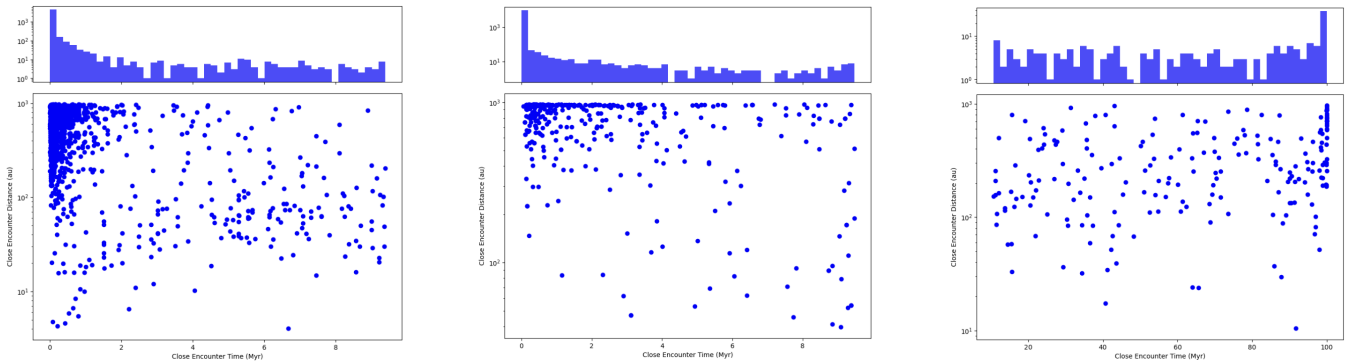

7 (a) 7 (b) 7 (c)

Figure 7. Figure 7(a), 7(b) and 7(c) illustrate the distribution of close encounter distance versus close encounter for a high-density environment till 10 Myrs, 10 to 100 Myrs and for low a density environment till 10 Myrs respectively.

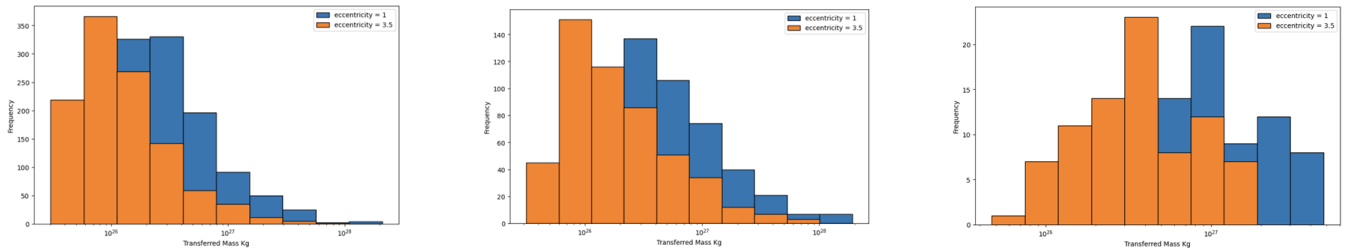

8 (a) 8 (b) 8 (c)

Figure 8. Figure 8(a), 8(b) and 8(c) illustrate the frequency of total mass transferred between stellar discs during an encounter. Figure 8(a) and 8(b) illustrates the mass transfer between stellar discs in a high density and low density environment respectively for the first 10 Myrs. The figure 8(c) illustrates the mass captured after 10 myrs till 100 myrs in a high density environment.

[h]

Time Interval (Myr)	High Density (eccentricity = 1)	High Density (eccentricity = 3.5)	Low Density (eccentricity = 1)	Low Density (eccentricity = 3.5)
0 – 2	1.04839×10^{23}	4.77818×10^{22}	4.05927×10^{22}	1.8484×10^{22}
2 – 4	2.38448×10^{22}	1.08278×10^{22}	2.21059×10^{22}	1.00279×10^{22}
4 – 6	7.97786×10^{21}	3.62038×10^{21}	8.70958×10^{21}	3.95197×10^{21}
6 – 8	9.68197×10^{21}	4.35581×10^{21}	9.32619×10^{21}	4.22609×10^{21}
8 - 10	1.64113×10^{22}	7.41027×10^{21}	3.21944×10^{22}	1.46299×10^{22}

Table 1. provides a detailed breakdown of no of rocky materials transferred time intervals, focusing on the influence of environmental density and eccentricity.

substantial number of 1.048390×10^{23} rocky materials in the initial 0–2 Myr interval. This value shows a significant reduction in the 2-4 Myr timeframe, dropping to 2.384480×10^{22} rocky materials. The subsequent intervals, 4-6 and 6–8 Myr, show relatively consistent values, with the latter slightly higher. The 8–10 Myr interval witnesses an increase, reaching 1.641138×10^{22} rocky materials. In contrast, the high-density environment with an eccentricity of 3.5 starts at 4.778182×10^{22} rocky materials in the 0–2 Myr interval, which is notably lower than its counterpart with an eccentricity of 1. This trend of reduced material transfer, relative to the eccentricity of 1, persists across all time intervals. The low-density environment, as expected, generally exhibits lower material transfer values than the high-density environment. For an eccentricity of 1, the material transfer starts at 4.059275×10^{22} rocky materials in the 0–2 Myr interval, with the 8–10 Myr interval showing a significant increase to 3.219448×10^{22} rocky materials. For an eccentricity of 3.5 in the low-density environment, the values are consistently lower across all time intervals when compared to an eccentricity of 1.

Graph 10 offers a compelling visualisation of the quantity of NR (the potentially biologically active rocky materials) transferred over an extended timescale of 10 to 100 million years. This analysis is specifically tailored to a high-density environment and examines two distinct eccentricities: 1 and 3.5. Upon analysing the graph, a clear trend emerges. Mirroring the patterns observed in mass transfer during a stellar encounter, the total count of rocks suitable for lithopanspermia exhibits a notable increase as the eccentricity of close encounters diminishes. This correlation underscores the profound influence of encounter eccentricity on the potential for transferring biologically viable materials between stellar systems and, hence, lithopanspermia. However, a critical caveat warrants attention. While the transfer of suitable rocks is evident over the 10- to 100-year timescale, their survival rate during this period is markedly low. This intriguing phenomenon, which raises questions about the longevity and resilience of these rocks amidst the vast expanse of space, will be the focal point of our discourse in the subsequent section.

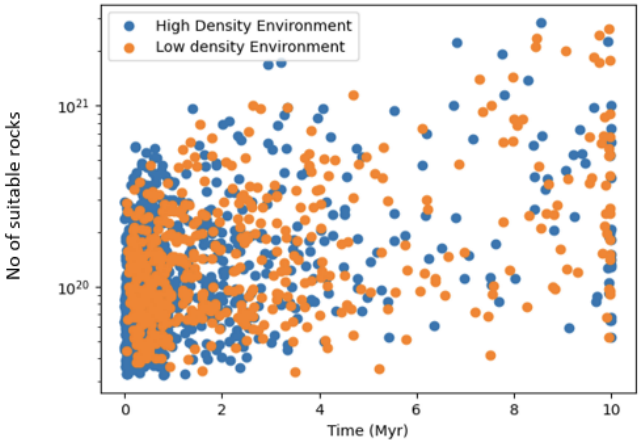

Figure 9. Plots the total number of rocky materials that are suitable to carry biologically active entities versus close encounter time.

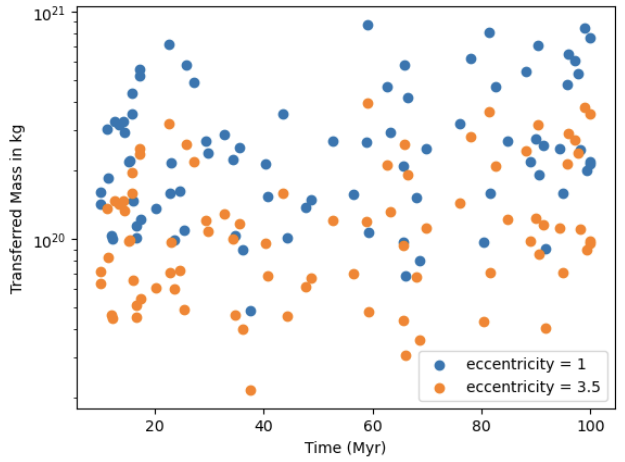

Figure 10. Plots the total number of rocky materials that are suitable to carry biologically active entities for an extended period of time from 10 to 100 Myrs for different eccentricities.

3.4 Mass transfer between binary stars during close encounter

In our simulations, we looked at about 50 binary stars. We explained how we found and counted these stars in the methods section. In this study, our main goal was to find out how much mass, especially rocks that might be able to carry life, moved between two binary star discs when they came close to each other.

What's interesting is that our results show no big difference in the amount of mass moved between binary stars (two stars together) and non-binary stars (just one star). This is surprising because you might think that two stars together would act differently. There could be many reasons for this. Maybe the way mass moves in binary stars is different than in non-binary stars. Or maybe there's something about binary stars that makes them act like non-binary stars when it comes to moving mass. It's also possible that other factors during these close meetings between stars make the results look the same, whether it's a binary or non-binary star .To better understand this, we'll need more studies in the future. It will help us learn more about how stars, whether they're on their own or in pairs, move mass around in space.

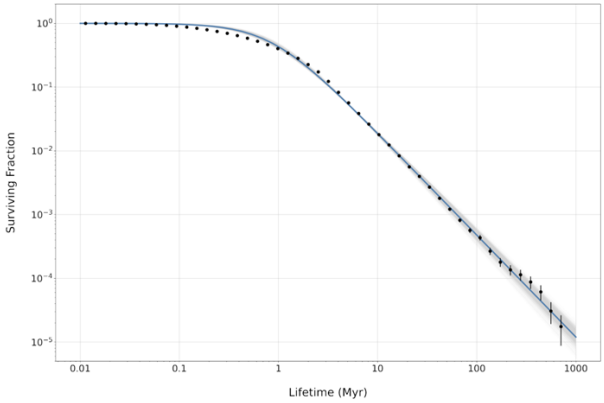

[H]

Figure 11. Gives us an idea of how many fractions of the transferred rocks will survive to the full duration of the simulation.

3.5 Fraction of materials at the end of the simulation

Delving deeper into the quantitative aspects of our simulations, we utilized the survival fraction equation, which is discussed in Section 2.6 under 'Methods'. By substituting the relevant values into this equation, we derived the following results:

- For the 10 Myr simulation: A mere 0.01865 fraction of the initially captured rocky materials persists after a span of 10 Myr.
- For the extended 100 Myr simulation: The survival fraction dwindles even further, with only 0.000477 of the captured materials enduring after 100 Myr.

These findings have profound implications for the concept of lithopanspermia as a potential life-transferring mechanism. The figure suggests that for life to be thriving in new celestial environments, the adaptation and growth processes must be set in motion almost immediately after the rocky materials are captured. As time advances, this probability of life thriving in the new celestial environment diminishes considerably. This temporal decline underscores the importance of the immediate aftermath of capture in the potential for life transfer via rocky debris. In essence, while the capture of interstellar objects is a crucial first step, the window for successful lithopanspermia is relatively narrow and decreases as time elapses.

3.6 Minimum disc radius for transfer

In the context of a circumstellar disc surrounding a star, a critical parameter emerges: the minimum disc radius, denoted as $r_{un,min}$. This radius is crucial because any potential mass transfer depends on $r_{un,min}$ being less than the standard disc radius of 100 astronomical units (au). The determination of this minimum disc radius is intricately tied to several factors. These include the proximity of the stars during their close encounters, their respective eccentricities, and their individual masses. This intricate relationship is visually represented in Graphs 12(a) and 12(b). These graphs plot the necessary minimum disc radius for mass transfer against varying close encounter distances and mass ratios. A closer examination of Graph 12(a), where the eccentricity is held constant at 0.5, reveals that the required minimum disc radius tends to be larger. Conversely, in Graph 12(b), with an eccentricity fixed at 3.5, the minimum disc radius is notably smaller. This observation implies that systems with a lower eccentricity will have fewer instances where $r_{un,min}$ is less than the stellar disc radius. However, the impact of eccentricity on

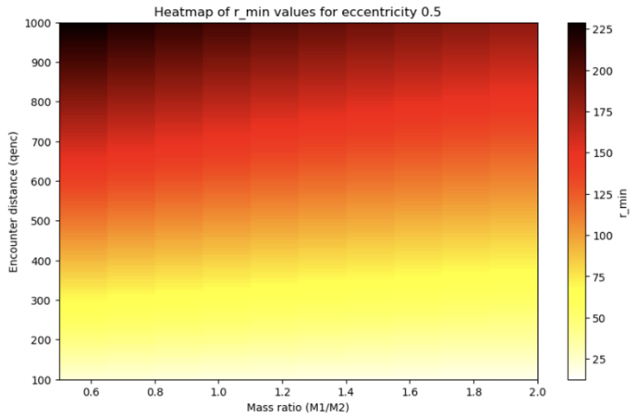

12 (a)

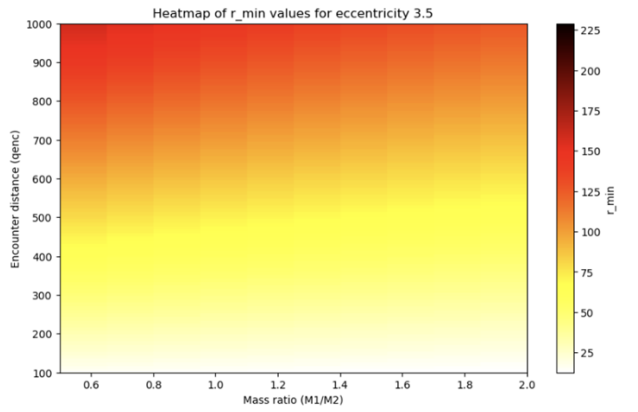

12 (b)

Figure 12. Figure 12(a) and 12 (b) plots the minimum disc radius for a number of close encounter distance values and mass ratios. Figure 12(a) depicts the minimum radius for transfer when eccentricity is 0.5 and 12 (b) depicts the minimum radius when eccentricity is 3.5. The close encounter distance and minimum radius for transfer are given in au

the minimum transfer disc radius is relatively weak (Jílková et al. 2016). Refer to Appendix C. The masses of the stellar discs and the distance of their close encounters exhibit a pronounced impact on the minimum transfer radius. This relationship is evident in both Graphs 12(a) and 12(b). Specifically, a shorter encounter distance and a higher mass ratio correlate with a reduced minimum transfer radius. As a result, stellar discs with these characteristics are more conducive to facilitating mass transfer.

3.7 Chain of encounters

Here we are presenting the results for multiple encounters as discussed in the method section. We present the details for the higher density environment and lower density environment. For a high density, We found that out of the total 1109 stars experiencing an encounter a total of 722 systems undergo multiple encounters. Out of this 722 multiple encounters there are encounters happening between 4 stars, 5 stars and so on. The table 1(a) below provides a detail of this multiple transfers in a high-density environment.

From table 2 and 3 it is clear that higher density environments have frequent multiple encounters, while in the case of lower density environments, the multiple encounters are less frequent. Therefore,

Table 2. Number of Systems involved in cascade of mass transfers and their frequencies in a high density environment

Number of Systems involved in encounter	Frequency
3	326
4	226
5	113
6	39
7	15
8	4
9	1

Table 3. Number of Systems involved in the cascade of mass transfers and their frequencies in a low density environment

Number of Systems involved in encounter	Frequency
3	120
4	40
5	15
6	11
7	2
8	1

with the increase in stellar density, the probability of lithopanspermia occurring between 3 or more star systems is also enhanced.

Statistically explaining, out of the 1109 star systems experiencing an encounter, multiple encounters occur in 65% of the systems in the case of a high-density environment. In contrast, in the case of a low-density environment, out of the 506 systems experiencing encounters, only 37% of the systems have multiple encounters.

From the frequency column of table 2 and 3 it is evident that there are multiple encounters where 4, 5, 6, 7, 8, and 9 stars are involved. This implies that the same biologically active rocks can be transferred between a number of systems. The mass transfer between systems in the case of multiple encounters will be chaotic. Measuring the mass transferred between multiple star systems is crucial and will help us understand the lithopanspermia events occurring between 3 or more stars.

4 DISCUSSION

In this research, we have calculated the amount of lithopanspermia events occurring when two stars are in close encounter. We have also measured how lithopanspermia varies with environments of different stellar densities. Additionally, we checked the dependency of mass transfer for two distinct close encounter eccentricities: when the eccentricity is 1 and when it is 3.5.

We found that in a higher density environment, the encounters are more frequent, leading to a higher number of mass transfers. Conversely, in a low-density environment, the encounters are less frequent, resulting in fewer lithopanspermia events. With respect to the dependency on eccentricity, mass transfer is more pronounced when the eccentricity is lower. Given our research objectives, we determined that the probability and possibilities of life transferring through the process of lithopanspermia are amplified in crowded environments and at lower encounter eccentricities.

In this research, we made a few assumptions to calculate mass transfer. The primary assumption is that life has already formed in the planetary systems, and we are gauging the efficiency of this mass

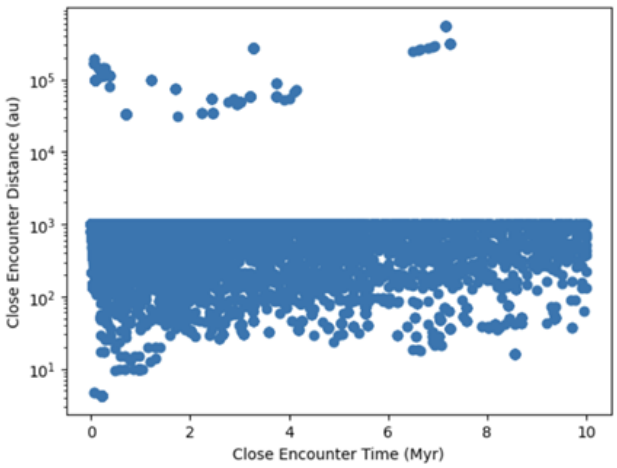

Figure 13. Plots the close encounter distance versus time showing the outliers in our close encounter distance data

transfer. Given that the planetary systems are already teeming with life, the rocks being transferred between stars are biologically active. Thus, we are effectively measuring the number of lithopanspermia events directly. Our second assumption is that the N-body simulation we run provides an accurate prediction of star formation and evolution. Details of the N-body simulations are provided in the method section. The mass transfer data is derived from the transfer efficiency graph of Jilkova et al. We assumed that this represents the transfer efficiency between stars during a close encounter.

4.1 Outliers in the dataset

The datasets we have analysed was obtained from the simulation run by my supervisor Richard Parker and the close encounter was set for less than 1000 au. The data set we analysed consist of few outliers and caveats. There are several stars with close encounter distance greater than 1000 au. Figure 13 plots the close encounter time in million years versus close encounter distance in au. As we can see from the figure there is several outliers lying at a close encounter distance greater than 1000 au, with some of them at a close encounter distance of 100000 au. Also, from the figure we also found that most of the close encounter is distributed at a close encounter distance of 1000 au which is another caveat. So while plotting the close encounter distance versus close encounter time we plot only those encounters happening below a close encounter distance of 990 au.

4.2 Outliers in the transfer efficiency prediction

The primary task of our research paper is to analyse the mass transfer occurring between stars during close encounters and this is obtained from the transfer efficiency figures of jilkova et al. We predicted the transfer efficiency for our data set from the values obtained from jilkova et al paper. While predicting the transfer efficiency values, we have one data point having negative transfer efficiency. This can be due to the model mismatch, thus predicting values outside the given range. We filter the data set by only taking transfer efficiency values larger than zero and thus ignoring the negative outlier. We do this for the transfer efficiency values for eccentricities 1 and 3.5.

4.3 Comparison

Our research focuses on the lithopanspermia events occurring between star systems. Several researchers have also calculated and estimated the number of lithopanspermia events. As previously mentioned, we have assumed that life has already formed in the star systems. However, this might not be the case in reality. Adams & Napier (2022) have conducted calculations and estimations regarding lithopanspermia events between planetary systems. Their findings suggest that while mass transfer between planetary systems is frequent, the likelihood of frequent lithopanspermia events is quite low. The biological aspects of the research, which involve estimating the probability of life being seeded on a planet and the subsequent probability of that life flourishing, remain uncertain. Adams and Napier determined that in a birth cluster, the number of captured rocks is 10^{11}, a figure substantially lower than our estimation of 10^{22}. This discrepancy arises because they considered a value of 10^{16} rocks per star, whereas our dataset assumes approximately 10^{26} rocks per star.

5 SUMMARY AND CONCLUSION

In a bid to understand the complexities of the cosmos, we embarked on an exploration of mass transfer between stellar systems during close encounters. Central to our research was the assumption that these stellar systems are biologically active. This assumption enables us to determine the number of lithopanspermia events and ascertain the efficiency of biologically active mass transfers.

We analyse star clusters across varying stellar densities: a high-density zone with a staggering 10^4 solar masses per cubic parsec, and a more modest low-density region with a stellar density of 100 solar masses per cubic parsec. The next phase of our investigation delves into the impact of eccentricities on this mass transfer. We compared results for eccentricities of both 1 and 3.5 across the two density areas. A clear pattern emerged: most mass transfers took place when the eccentricity was at its lowest. Additionally, the higher the stellar density, the greater the frequency of close encounters and, by extension, mass transfers.

We then consider the case when the mass transferred can or cannot be biologically active. Using this assumption, we were able to estimate the amount of rocky material capable of ferrying biologically active entities. The trends observed in mass transfer were mirrored here too: a direct correlation was seen where higher densities resulted in increased transfers of rocky materials.

While our initial simulations focused on the first 10 million years, we expanded our horizons to encompass a period up to 100 million years. We saw a drop in the number of close encounters, and hence mass transfers. Despite the drop in close encounters over this extended timeframe, the peak of mass transfer remained consistent with our earlier observations from 0–10 million years ago. This signalled that the majority of these disc interactions took place in the first few million years and, hence, in young star clusters.

We then measured how much of this transferred mass would survive at the end of the simulation. We found that with time, the survivability fraction of rocky materials decreases, meaning that after the mass transfer, for a biological entity to grow on the new planet, it should happen quickly.

The spatial dimensions of our research can be found in the "disc" regions of star systems, recognised as planetary cradles. We established a baseline or minimum disc radius, signifying the necessary conditions for successful mass transfers. In essence, a star's disc radius needs to exceed this minimum disc radius for a transfer to occur.

Finally, we found the systems that undergo chain encounters. This refers to sequences of engagements where numerous systems participate, resulting in a cascade of mass transfers. Surprisingly, a vast number of systems experienced these chain encounters, signifying a picture of a star cluster where mass is consistently transferred between multiple stellar systems.

Our study concludes that mass transfers between stellar discs during close encounters are a frequent phenomenon. By assuming that these stellar systems are biologically active from the outset, we were able to calculate the lithopanspermia events and the mass of materials transferred in such instances. This provides pivotal insights into possible lithopanspermia events, should these systems indeed harbour life.

However, it's essential to note the current limitations. As of now, with our existing technological capabilities and knowledge, directly observing biologically active entities within stellar clusters remains a daunting challenge. Yet, our research underscores the probability of mass transfers between stellar discs. As technology continues to evolve and our observational methods become increasingly refined, we remain hopeful that future investigations will shed light on the actual occurrence of lithopanspermia. Determining whether life has indeed journeyed between stellar systems would mark a monumental leap in both astrobiology and astrophysics.

ACKNOWLEDGEMENTS

First and foremost, I express my profound gratitude to the almighty God for bestowing upon me the health and wisdom to bring this research project successful. I am deeply indebted to my supervisor, Dr. Richard J. Parker, for his invaluable guidance, insights, and unwavering support that were instrumental in the successful completion of this project. My heartfelt thanks also go to my colleagues and flatmates, whose constructive feedback greatly enhanced the quality and context of this work.

DATA AVAILABILITY

The simulation data set used for this research study was obtained from my supervisor Dr. Richard J.Parker. The analysis and calculation were conducted in Python using Jupyter Notebook. The data used for calculating the mass transfer for our dataset was obtained from Figure 8 and Figure 9 of Jílková et al. (2016). The important and complicated Python codes used in this study are given in the appendix.

REFERENCES

Adams F. C., Napier K. J., 2022, Astrobiology, 22, 1429
Adams F. C., Spergel D. N., 2005, Astrobiology, 5, 497
Belbruno E., Moro-Martín A., Malhotra R., Savransky D., 2012, Astrobiology, 12, 754
Chen H., Forbes J. C., Loeb A., 2018, The Astrophysical Journal Letters, 855, L1
Crick F. H., Orgel L. E., 1973, Icarus, 19, 341
Dehnen W., Read J. I., 2011, The European Physical Journal Plus, 126, 1
Eubanks T. M., et al., 2021, arXiv preprint arXiv:2103.03289
Gobat R., Hong S. E., Snaith O., Hong S., 2021, The Astrophysical Journal, 921, 157
Goodwin S. P., Whitworth A. P., 2004, Astronomy & Astrophysics, 413, 929
Horneck G., 1993, Origins of Life and Evolution of the Biosphere, 23, 37
Horneck G., Bücker H., Reitz G., 1994, Advances in Space Research, 14, 41
Jílková L., Hamers A. S., Hammer M., Portegies Zwart S., 2016, Monthly Notices of the Royal Astronomical Society, 457, 4218
Maschberger T., 2013, Monthly Notices of the Royal Astronomical Society, 429, 1725
McKay D. S., et al., 1996, Science, 273, 924
Meech K. J., et al., 2017, Nature, 552, 378
Melosh H. J., 2003, Astrobiology, 3, 207
Pang X., et al., 2023, The Astronomical Journal, 166, 110
Parker R. J., 2014, Monthly Notices of the Royal Astronomical Society, 445, 4037
Parker R. J., 2020, Royal Society Open Science, 7, 201271
Rampelotto P. H., 2010, in Astrobiology Science Conference 2010: Evolution and Life: Surviving Catastrophes and Extremes on Earth and Beyond. p. 5224
Rice W., Lodato G., Pringle J., Armitage P., Bonnell I. A., 2004, Monthly Notices of the Royal Astronomical Society, 355, 543
Secker J., Wesson P. S., Lepock J. R., 1996, arXiv preprint astro-ph/9607139
Wesson P. S., 2010, Space Science Reviews, 156, 239
Worth R. J., Sigurdsson S., House C. H., 2013, Astrobiology, 13, 1155

APPENDIX

Appendix A: Code used to measure the transferred mass

We used a linear regression model to calculate the total transferred mass, the python code used for this is given below:

```
#Importing libraries and models
from sklearn.linear_model import LinearRegression
#Transfer efficiency data of Jilkova et al, when ecc = 1
df1 = pd.read_csv("C:\Ahzam\MSc Astrophysics\Project\Python\data's\mass vs encounter distance\e = 1.csv")

# create the model
model = LinearRegression()

# training the model on jilkova et al data values
X_train = df1[['Mass_ratio', 'Qenc']]
y_train = df1['transfer_efficiency']
model.fit(X_train, y_train)

# using the model to predict transfer efficiency for our dataset
X_test = star_transfer[['Mass_ratio', 'Qenc']]
y_pred = model.predict(X_test)
#y_pred consists of transfer efficiency values of our data set.
```

In the code provided, we utilized the `linearRegression` module from `sklearn`. The variable `df1` represents the data values obtained from the paper by Jílková et al. (2016). The `star_transfer` dataset comprises our mass ratio and close encounter distance values. We trained the model using this data and subsequently employed the trained model to predict the transfer efficiency of our dataset.

Appendix B: Code used to find the chain of encounters

We found the systems that undergo a chain or cascade of encounters by constructing a loop using python the code used is given below:

```
#Importing libraries and models
from sklearn.linear_model import LinearRegression
#Transfer efficiency data of Jilkova et al, when ecc = 1
df1 = pd.read_csv("C:\Ahzam\MSc Astrophysics\Project\Python\data's\mass vs encounter distance\e = 1.csv")

# create the model
model = LinearRegression()

# training the model on jilkova et al data values
X_train = df1[['Mass_ratio', 'Qenc']]
y_train = df1['transfer_efficiency']
model.fit(X_train, y_train)

# using the model to predict transfer efficiency for our dataset
X_test = star_transfer[['Mass_ratio', 'Qenc']]
y_pred = model.predict(X_test)
#y_pred consists of transfer efficiency values of our data set.
```

The code starts by importing the `Pandas` library and then initializes an empty `DataFrame` named `results_df` to store results, with columns 'Particle ID' and 'Chain of Encounters'. Next, it forms a dictionary, `encounter_dict`, from the `star_transfer_possible` DataFrame. This dictionary links particle IDs to the stars they encounter. The `star_transfer_possible` is the dataset we aim to analyze.

A function named `trace_encounter_chain` is then defined to trace a sequence (or chain) of encounters, starting from any given

particle ID. This function goes through the encounters listed in the `encounter_dict` and continues until it either spots a repeated encounter (indicating a loop) or can't find any more encounters.

After defining this function, the code reviews every unique particle ID in the `star_transfer_possible` DataFrame. For each ID, it maps out its sequence of encounters using the `trace_encounter_chain` function. The sequence, together with the particle ID, is then added to the `results_df` DataFrame.

The code finishes by displaying the complete `results_df`, which shows the encounter sequence for each particle.

Appendix C

Dependency of eccentricity on minimum transfer radius is analyzed. We found that the eccentricity only weakly influences the minimum transfer radius. This is evident from the below graph.

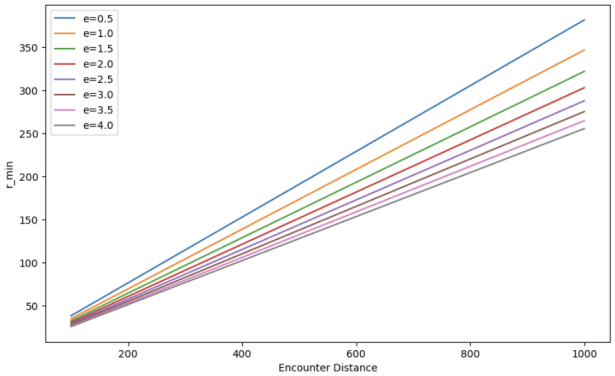

In the above Figure minimum transfer radius and close encounter distance are given in au. from the figure it is evident that minimum transfer radius only increases slightly with the decrease in eccentricity. While considering the influence of mass ratio and close encounter distance on minimum transfer radius the effect of eccentricity on minimum transfer radius is almost negligible.

This paper has been typeset from a TEX/LATEX file prepared by the author.